

Stochastic Computing Implemented by Skyrmionic Logic Devices

Haoyang Zhang^{1,2&}, Daoqian Zhu^{1,2&}, Wang Kang^{1,2*}, Youguang Zhang³, Weisheng Zhao^{1,2*}

¹Fert Beijing Research Institute, BDBC, Beihang University, Beijing 100191, China

²School of Microelectronics, Beihang University, Beijing, 100191, China.

³School of Electronics and Information Engineering, Beihang University, Beijing 100191, China

[&]These authors contributed equally to this work

*E-mails: wang.kang@buaa.edu.cn and weisheng.zhao@buaa.edu.cn

Abstract

Magnetic skyrmions, topologically non-trivial spin textures, have been considered as promising information carriers in future electronic devices because of their nanoscale size, low depinning current density and high motion velocity. Despite the broad interests in skyrmion racetrack memory, researchers have been recently exploiting logic functions enabled by using the particle-like behaviors of skyrmions. These functions can be applied to unconventional computing, such as stochastic computing (SC), which treats data as probabilities and is superior to binary computing due to its simplicity of logic operations. In this work, we demonstrate SC implemented by skyrmionic logic devices. We propose a skyrmionic AND-OR logic device as a multiplier in the stochastic domain and two skyrmionic multiplexers (MUXs) as stochastic adders. With the assistance of voltage controlled magnetic anisotropy (VCMA) effect, precise control of skyrmions collision is not required in the skyrmionic AND-OR logic device, thus high thermal stability can be achieved. In the two MUXs, skyrmions are driven by Zhang-Li torque or spin orbit torque (SOT). Particularly, we can flexibly regulate the

skyrmion motion by VCMA effect or voltage controlled Dzyaloshinskii-Moriya Interaction (VCDMI) effect in the SOT-driven case. In our design, an 8-bit stochastic multiplier and an adder are further verified by micromagnetic simulations, which are competitive in terms of time efficiency and energy cost in comparison with typical CMOS based stochastic circuits. Our work opens up a new route to implement SC using skyrmionic logic devices.

I. INTRODUCTION

Magnetic skyrmions are topologically stable chiral structures, which are generated at the B20-type bulk materials or ultra-thin ferromagnetic (FM) layers favored by Dzyaloshinskii-Moriya Interaction (DMI) [1-6]. Due to their small size, high motion velocity and low depinning current density, skyrmions have been considered as promising carriers to transfer information in future electronic devices [7-10]. Over the past years, much effort has been devoted in developing skyrmion based racetrack memory [11-16], which requires no mechanical parts and shows great potential in advanced high-density storage applications. Moreover, by exploiting the particle-like behaviors of skyrmions, logic device concepts with high operation speed and low power consumption have also been proposed.

One of the most essential application of skyrmionic logic device is to support stochastic computing (SC), which can be realized by AND and multiplexer (MUX) logic operations. SC is an unconventional computing method that treats data as probabilities [17-19]. A N -bit stochastic number (SN) bit-stream with X 1s denotes a probability of $P = X/N$, indicating the probability of observing bit 1 at a bit-stream. SC has been applied in the massively parallel computing system for its good tolerance to soft errors as well as high operation speed [20]. Besides, SN and X are flexible, which brings great convenience to its applications. To date, SC has been typically implemented in CMOS based stochastic circuits, which suffers from the challenges of power consumption and area cost [21-22]. Skyrmionic logic devices emerge as a solution to these issues. However, the existing proposals of skyrmionic AND logic

devices encounter low room temperature stability due to the narrow width of the racetrack and the requirement to precisely control skyrmions collision to execute logic operations [8, 23]. In addition, no skyrmionic MUX has been proposed yet.

In this work, we propose a skyrmionic AND-OR logic device and two types of skyrmionic MUXs regarding the skyrmions motion manner to implement SC. In the skyrmionic AND-OR logic device, which acts as a stochastic multiplier [24] in SC, skyrmions are driven by spin orbit torque (SOT) [25-27] and guided by voltage controlled magnetic anisotropy (VCMA) effect [28-30]. Therefore, it is not necessary to accurately control skyrmions collision to execute logic operations and this device can tolerate the thermal diffusion under $T = 250$ K. In the skyrmionic MUXs operating as a stochastic adder [24], skyrmions can be driven by Zhang-Li torque or SOT. VCMA effect or voltage controlled DMI (VCDMI) effect [31] is used to dynamically modify the energy landscape to regulate the skyrmion motion in such devices. Based on the above single-bit logic device, 8-bit SN stochastic multiplier and stochastic adder are further confirmed by micromagnetic simulations. Subsequently, the performance of the proposed skyrmionic logic devices is analyzed, which shows broad prospects on implementing SC compared to typical CMOS based stochastic circuits.

II. Skyrmionic AND-OR Logic Device

In the proposed structure shown in Fig. 1(a), the skyrmionic AND-OR device is mainly composed of three parts, including heavy metal (HM) layer, ferromagnetic (FM) layer and two electrode gates. The HM layer, which is beneath the FM layer (not shown in the figure), is used for the flow of driving current to drive skyrmion from the left side to the right side by the spin Hall effect [32]. We apply positive voltages on electrode gate 1 (V_{g1}) and 2 (V_{g2}) (see Fig.1(b)), increasing the potential energy of the FM layer beneath V_{g1} and V_{g2} to guide the skyrmion motion. The effect of a voltage V on the perpendicular magnetic anisotropy (PMA) [33] can be calculated by the equation $K_g = K_u + \zeta \cdot V / (d \cdot h)$, where the VCMA coefficient ζ is set as $48 \text{ fJ} \cdot \text{V}^{-1} \cdot \text{m}^{-1}$ according to previous reports [29], d denotes the thickness of the insulator layer between electrode gates and the FM layer, and h is the thickness of the FM layer, which are both set as 1

nm in our simulations. Precisely, if a +2 V voltage is applied on one electrode gate, the PMA of the FM layer beneath it will increase from $0.8 \text{ MJ}\cdot\text{m}^{-3}$ to $0.896 \text{ MJ}\cdot\text{m}^{-3}$, creating an energy barrier blocking the skyrmions from crossing this region.

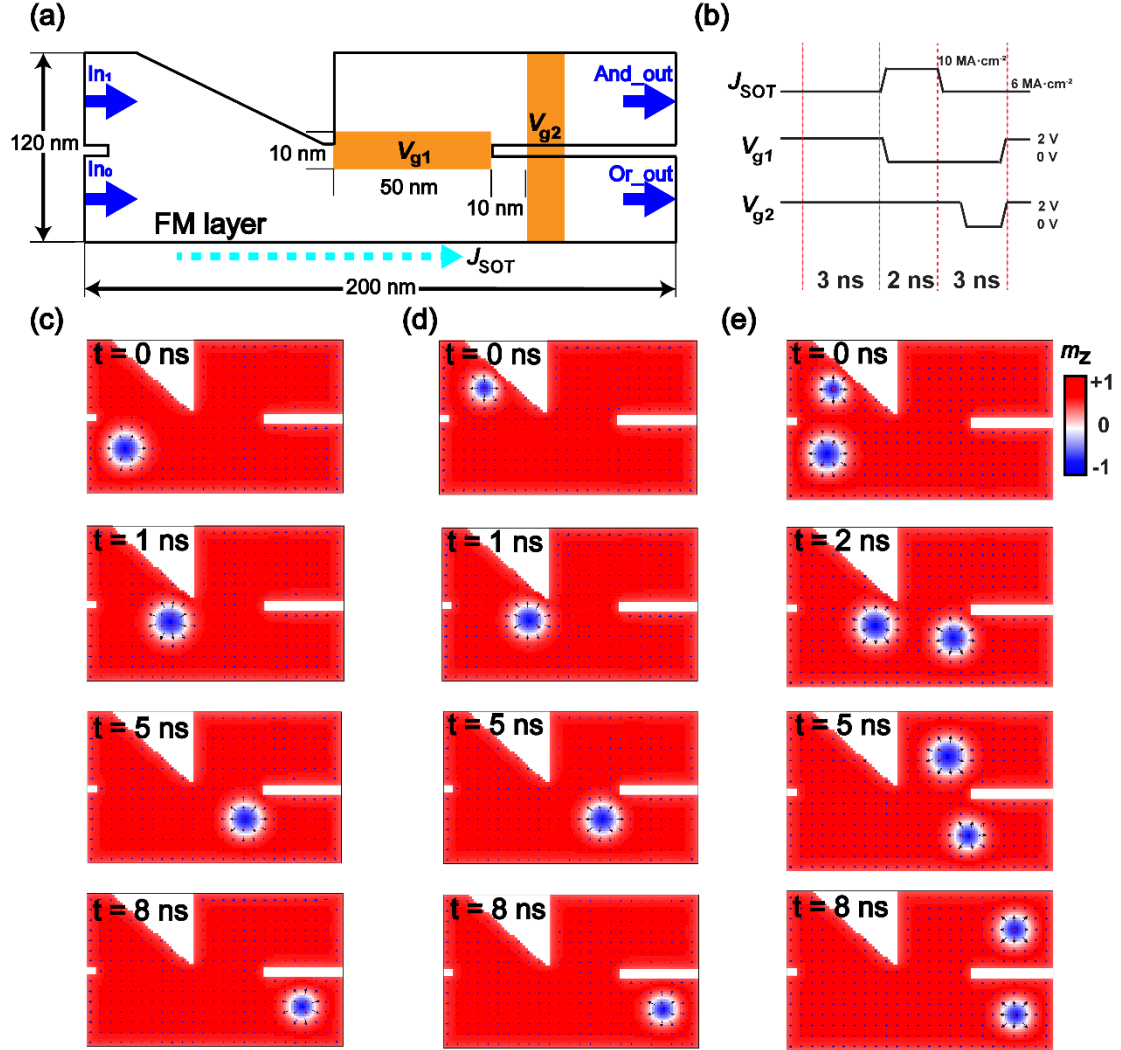


FIG. 1 Skyrmionic AND-OR logic device at $T = 0 \text{ K}$. (a) Device structure with two input lanes and two output lanes. The two electrode gates (V_{g1} , V_{g2}) are designed to modulate the skyrmion motion through the VCMA effect. (b) Profile of the SOT current density (J_{SOT}) and applied positive voltages to achieve the device function. (c-e) Three cases of the inputs and their corresponding simulation processes and outputs. In the snapshots of micromagnetic simulations, red region represents spin up ($m_z = +1$), blue represents spin down ($m_z = -1$) and white represents spin that horizontal to the plane ($m_z = 0$).

Fig. 1(b) shows the profile of the SOT current density (J_{SOT}) and the electrode voltages to achieve the device function. A voltage of +2V is dynamically applied on V_{g1} and V_{g2} to guide the skyrmions motion. Fig.1(c-e) demonstrates the top-viewed

simulation snapshots under three different inputs. The data “1” or “0” is encoded by the presence or absence (in FM background) of a skyrmion. In the circumstance with only one skyrmion input, this skyrmion will enter OR lane and be blocked at a position near V_{g2} under the joint effect of VCMA, $J_{\text{SOT}} = 6 \text{ MA} \cdot \text{cm}^{-2}$ for 3 ns and repulsion from the edge [34-35]. After the positive voltage on V_{g2} is removed, the skyrmion finally outputs from the OR lane. Therefore, the OR and AND lane generate an output of “1” and “0”, respectively. In the case with two skyrmion inputs, the first skyrmion (from In_0) stops near V_{g2} , similar to the aforementioned behavior. The subsequent skyrmion (from In_1) is then blocked because of the repulsion from the first skyrmion and the energy potential caused by V_{g1} . At $t = 3 \text{ ns}$, the voltage on V_{g1} is set to 0 V and J_{SOT} increases to $10 \text{ MA} \cdot \text{cm}^{-2}$. Thus, the subsequent skyrmion will be driven to the AND lane by a combined effect of skyrmion Hall Effect [36-40], skyrmion-skyrmion repulsion and skyrmion-edge repulsion while the first skyrmion moves out from OR lane after the voltage on V_{g2} returns to 0. In this case, both OR and AND lane give rise to an output of data “1”. Obviously, AND-OR logic function is realized in our proposed device. Note that during these operations, it is not necessary to precisely control the skyrmion-skyrmion collision. However, in the previous proposals [8, 23], this is required to realize logic function, which will suffer from instability in the presence of thermal effect and pinning. We further verify the function of the proposed AND-OR Logic device at $T = 250 \text{ K}$ (See Appendix B for details), indicating the higher thermal stability of our device.

Moreover, we designed an 8-bit stochastic multiplier, using the proposed single-bit skyrmionic logic AND-OR device as the stochastic multiplier cell. Fig. 2(a) shows the schematic of multiplication computation of $4/8 \times 6/8$ implemented by an AND logic gate, which can be physically achieved with our proposed skyrmionic device, as exhibited in Fig. 2(b). The AND function is implemented using the above single-bit skyrmionic logic AND-OR device while the inputs and outputs can be stored in the corresponding elongated lanes. Notches at the lanes are used to synchronize the input and output skyrmions, and to divide each lane into 8 regions (yellow regions in Fig. 2(b)). Through periodically increasing the current to $J_{\text{SOT}} = 20 \text{ MA} \cdot \text{cm}^{-2}$ for 0.6 ns, skyrmions can move to the region of the next data bit [23]. Otherwise, skyrmions will

be blocked in their original area. The operation timing diagram of a single-bit AND-OR logic operation in one cycle is shown in Fig. 2(c). Compared to the timing diagram in Fig. 1(b), an additional 0.6 ns wide high current pulse is provided every 19.6 ns to synchronize the skyrmions, which means that the whole operation time for 8-bit multiplication computing is about 156.8 ns. In our simulations, input skyrmions are initialed at the left racetracks. There are four and six skyrmions distributed in the two 8-bit input lanes, denoting two probabilities of $P_1 = 4/8$ and $P_0 = 6/8$, respectively. After eight cycles of single-bit operation, three skyrmions output from the AND lane, as shown in Fig. 2(d), illustrating an output probability of $P_{\text{out}} = 3/8$ and the capableness of our device to perform stochastic multiplication.

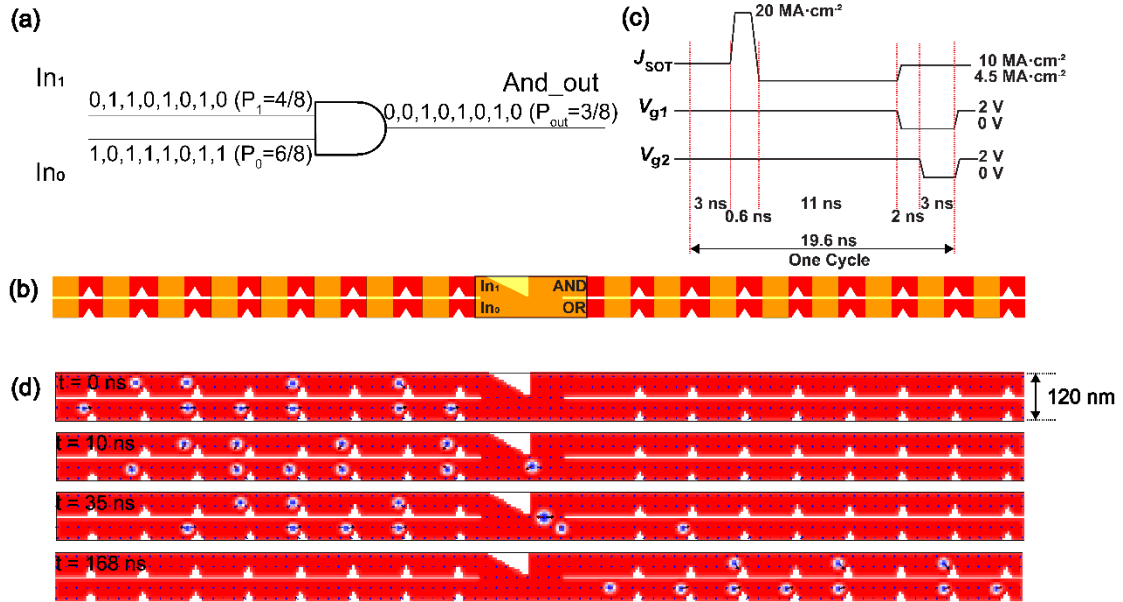


FIG. 2 Skyrmionic AND-OR logic device used as an 8-bit stochastic multiplier. (a) Schematic of an exact multiplication computation of $4/8 \times 6/8 = 3/8$. A logic AND gate is required during the operation. (b) Schematic of the proposed 8-bit skyrmionic stochastic multiplier. Notches are used to divide each lane into 8 regions and to synchronize the motion of skyrmions. (c) Profile of driving current density (J_{sot}) and electrode voltages in a single-bit operation cycle. (d) Snapshots of the magnetization configuration of the 8-bit stochastic multiplier at selected times. At $t = 0$ ns, the skyrmions distributed in the two input lanes represent probabilities $P_1 = 4/8$ and $P_0 = 6/8$, respectively. After 168 ns, AND lane will output the binary sequence of “0, 0, 1, 0, 1, 0, 1, 0”, i.e., a probability of $P_{\text{out}} = 3/8$, which denotes the multiplication result of two inputs.

III. Skyrmionic MUXs

Addition operation in SC can be performed by a MUX [24], where two input bit-streams (In_1 , In_0) are selected by a select signal S with a probability of 0.5, thus the output bit-stream owns a probability that is half sum of the two inputs. Considering the feature of a MUX and the particle-like behaviors of skyrmions, we propose two types of skyrmionic MUXs regarding the skyrmion motion manner.

Fig. 3(a) shows the first scheme to implement the MUX logic, which is based on the deflection of skyrmions at an interface between regions with different DMI. The DMI constant D_1 of the left side is set as $3.5 \text{ mJ}\cdot\text{m}^{-2}$ while D_2 of the right plane varies from 3.35 to $3.65 \text{ mJ}\cdot\text{m}^{-2}$. The skyrmion deflection direction depends on the relative magnitude of D_1 and D_2 . Specifically, in our settings, if $D_2 > D_1$, skyrmions will be deflected along $+y$ direction. Therefore, skyrmions from In_0 will enter the OUT lane while skyrmions from In_1 will output from the C_1 lane, which means data from In_0 is selected. In contrast, if $D_2 < D_1$, skyrmions from In_1 will enter the OUT lane, while skyrmion from In_0 will crush at the lower edge. By regulating D_2 through VCDMI effect according to a select signal S , MUX logic can be implemented in our device. Note that when skyrmions cross the interface where the DMI changes, the applied in-plane polarized current (CIP) J_{STT} maintains $-15 \text{ MA}\cdot\text{cm}^{-2}$ (see Fig. 3(b)). If the current density is too high, skyrmions will quickly go through the interface, leading to a small displacement along y direction, not enough to realize the function.

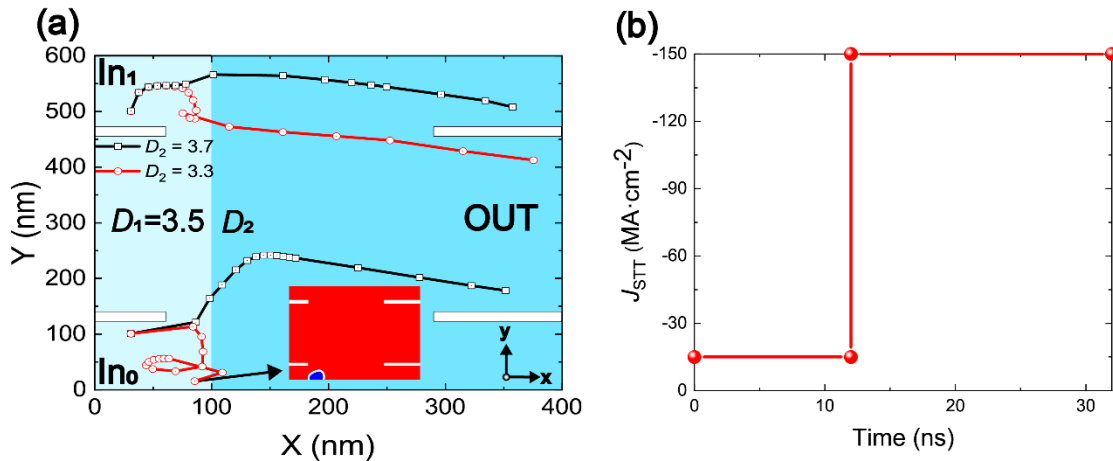


FIG. 3 Skymionic MUX driven by the Zhang-Li torque. (a) Schematic of the proposed device, where the DMIs in the left panel (D_1) and right panel (D_2) are different. There are two input lanes (In_0, In_1), one output lane (OUT) to export the selected data. Trajectories of skyrmions are indicated by the black and red symbols when $D_2 = 3.35$ or $3.65 \text{ mJ}\cdot\text{m}^{-2}$ while D_1 is fixed as $3.5 \text{ mJ}\cdot\text{m}^{-2}$. (b) Profile of the driving in-plane polarized current J_{STT} . Note that a damping constant $\alpha = 0.1$ is used in the simulations of (a) to obtain large enough skyrmion deflection.

However, this scheme has several shortcomings. First, the stability and the power efficiency of this device will be affected by the crush of skyrmions. Second, deflection toward $-y$ direction at the interface can only be achieved when skyrmions are driven by the Zhang-Li torque (See Appendix C for the simulation results of SOT-driven case and Discussion for explanation), which consumes more energy and time than the SOT-driven case. In addition, the skyrmion displacement along the y direction is inversely proportional to the damping constant [41], which indicates that the damping constant should be relatively low ($\alpha = 0.1$ is used in this simulation) to enable an enough displacement. However, in the widely studied Pt/Co system, damping is usually larger than 0.1 [42].

Therefore, we propose another scheme of skymionic MUX where skyrmions are driven by SOT. There are two copy lanes (C_1, C_0) outputting the data that is not selected by S. As shown in Fig. 4(a), an oblique interface is introduced to guide the skyrmion motion. Three electrode gates (V_{G1}, V_{G2}, V_{G3}) are used to lower the DMI value of the FM layer beneath the electrode gates through the VCDMI effect [31]. V_{G1} and V_{G3} are always applied with the same voltage, which are used to select the input skyrmion from In_1 . By contrast, a voltage different from V_{G1} and V_{G3} is applied on V_{G2} to select skyrmion from In_0 . The select signal S can be produced by a random number generator (RNG) [43-45], where the probability of “1” is 0.5. When the random number from S is 0, D_2 will decrease to $3.2 \text{ mJ}\cdot\text{m}^{-2}$, creating a high energy barrier to guide skyrmions from In_0 to enter the OUT lane. In the meantime, D_1 and D_3 remain unchanged (default value $D = 3.5 \text{ mJ}\cdot\text{m}^{-2}$). Therefore, skyrmions from In_1 will output from C_1 . When the random number is 1, only V_{G1} and V_{G3} are selected, lowering D_1 and D_3 to $3.2 \text{ mJ}\cdot\text{m}^{-2}$ simultaneously. Therefore, skyrmions from In_1 eventually move to the OUT lane while

skyrmions from In_0 are guided by V_{G3} and enter the C_0 lane. The trajectories of skyrmions under different situations are explicitly shown in Fig. 4(a).

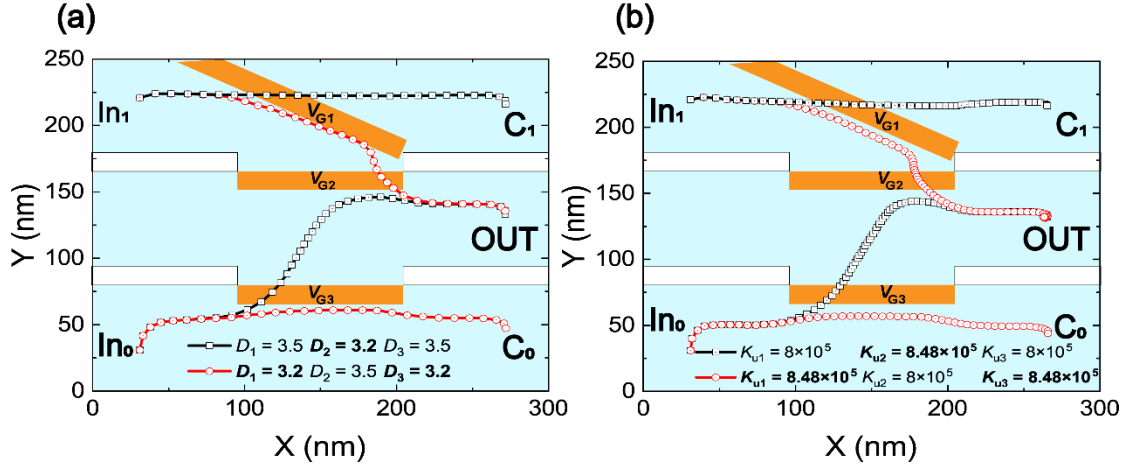


FIG. 4 Skyrmionic MUXs driven by the SOT. Schematic of the proposed device, where the energy landscape is dynamically changed through (a) VCDMI effect (b) VCMA effect. Three electrode gates (V_{G1} , V_{G2} , V_{G3}) are introduced to guide the skyrmion motion. Trajectories of the skyrmions are indicated by the black and red lines when selecting data from different lanes. J_{SOT} applied in (a) and (b) is $6.1 \text{ MA}\cdot\text{cm}^{-2}$ and $4.0 \text{ MA}\cdot\text{cm}^{-2}$, respectively.

During the operation, the $0.3 \text{ mJ}\cdot\text{m}^{-2}$ difference of DMI can sustain a max current density of $J_{SOT} = 6.1 \text{ MA}\cdot\text{cm}^{-2}$. If the current is higher, skyrmions from In_1 will go through the V_{G1} region and enter the C_1 lane, leading to the wrong logic output. Except for VCDMI, VCMA effect can also be used to change the local potential energy. Fig. 4(b) shows the schematic of a skyrmionic MUX using the VCMA effect. Like Fig. 4(a), three voltage gates are placed to modify the energy landscape in the device. In our simulations, we apply a +1 V voltage on the electrode gates to increase the local PMA energy density from $0.8 \text{ MJ}\cdot\text{m}^{-3}$ to $0.848 \text{ MJ}\cdot\text{m}^{-3}$. In this case, the max current density is $J_{SOT} = 3.0 \text{ MA}\cdot\text{cm}^{-2}$, otherwise skyrmions will enter wrong lanes. Materials with higher VCMA coefficient or higher voltages can be used to improve the device speed.

Based on the single-bit MUX device using the VCMA effect, we further design an 8-bit stochastic adder. Fig. 5(a) is the schematic of an exact addition computation of $1/2 \cdot (7/8 + 3/8)$ performed by a MUX. The structure of the proposed 8-bit skyrmionic stochastic adder is shown in Fig. 5(b). Following the timing diagram in Fig. 5(c), the proposed skyrmionic MUX can select the skyrmion from In_1 or In_0 depending on the

sequence S produced by a RNG. Like the 8-bit stochastic multiplier, a high current $J_{\text{SOT}} = 10 \text{ MA}\cdot\text{cm}^{-2}$ for 2.2 ns is used every 17.2 ns to enable skyrmions cross the notches and to synchronize the skyrmions. Therefore, the whole duration to complete the 8-bit MUX logic operation is 137.6 ns. Fig. 5(d) shows the snapshots of the magnetization configuration at selected times. We can find that there are five skyrmions on the 8-bit OUT lane, denoting a probability of $P_{\text{out}} = 5/8$, which is exactly the half sum of the two input probabilities of $P_1 = 7/8$ and $P_0 = 3/8$.

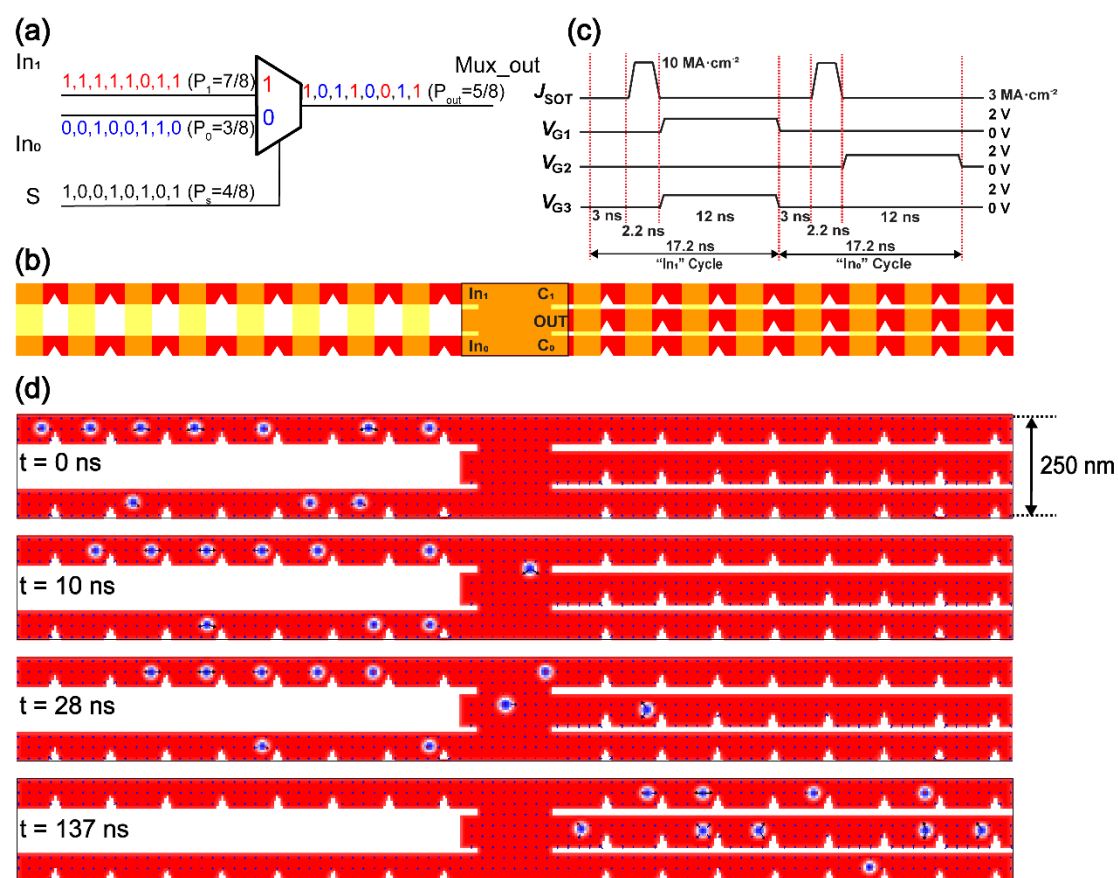


FIG. 5 Skyrmionic MUX used as an 8-bit stochastic adder. (a) Schematic of an exact addition computation of $\frac{1}{2} \cdot (\frac{7}{8} + \frac{3}{8}) = \frac{5}{8}$ implemented by a MUX. (b) Schematic of the proposed 8-bit stochastic adder. (c) Profile of the driving current density (J_{SOT}) and the applied voltages on three electrode gates (V_{G1} , V_{G2} , V_{G3}) in a single-bit operation cycle. (d) Snapshots of the magnetization configuration of the 8-bit stochastic multiplier at selected times. At $t = 0 \text{ ns}$, the skyrmions distributed in the two input lanes represent probabilities $P_1 = 7/8$ and $P_0 = 3/8$, respectively. After 137 ns, the OUT lane will output the binary sequence of “1, 0, 1, 1, 0, 0, 1, 1”, i.e., a probability of $P_{\text{out}} = 5/8$, which denotes the half sum result of two inputs.

IV. Discussion

A. Skyrmion dynamics at an interface where DMI changes

To understand the skyrmion dynamics in the two proposed MUXs, we investigate the trajectory of skyrmions driven by the Zhang-Li torque or SOT based on the Thiele equation which assumes that skyrmions are rigid during the steady motion.

We first analyze the skyrmion dynamics driven by the Zhang-Li torque. The Thiele equation for this case reads [46]:

$$\mathbf{G} \times (\mathbf{v} - \mathbf{u}) - \alpha D \mathbf{v} + \mathbf{F}_i = 0 \quad (1)$$

Here, $\mathbf{G} = (0, 0, G)$ is the gyromagnetic coupling vector, where $G = \frac{M_s t_F}{\gamma} 4\pi Q$ with saturation magnetization M_s , FM layer thickness t_F , gyromagnetic ratio γ , and skyrmion number $Q = -\frac{1}{4\pi} \iint \mathbf{m} \cdot \left(\frac{\partial \mathbf{m}}{\partial x} \times \frac{\partial \mathbf{m}}{\partial y} \right) dS$; $\mathbf{v} = (v_x, v_y, 0)$ is skyrmion motion velocity; \mathbf{u} is a vector along the electron motion direction with amplitude u ; α is the damping constant; $D = \frac{M_s t_F}{\gamma} \iint \left(\frac{\partial \mathbf{m}}{\partial x} \right)^2 dS$ is the dissipative force; $\mathbf{F}_i = -\nabla V(\mathbf{r})$ is the force induced by the interface where DMI changes with $V(\mathbf{r})$ denoting the system energy when a skyrmion locates at position \mathbf{r} . Assume that we apply an in-plane current along $-x$ direction and the interface is exactly along y direction as shown in Fig. 3(a), the solution to Eq. (1) is given by:

$$\begin{cases} v_x = \frac{\alpha D F_i + G^2 u}{G^2 + (\alpha D)^2} \\ v_y = \frac{G(F_i - \alpha D u)}{G^2 + (\alpha D)^2} \end{cases} \quad (2)$$

where F_i denotes the magnitude of the force \mathbf{F}_i .

If $D_1 = D_2$ or skyrmions are far away enough from the interface, we can set $F_i = 0$ in Eq. (2). As a consequence, we obtain $v_x = \frac{G^2 u}{G^2 + (\alpha D)^2}$ and $v_y = \frac{-\alpha D G u}{G^2 + (\alpha D)^2}$. This illustrates that skyrmions will gain a velocity along $+x$ direction in this case, which is the feature of the Zhang-Li torque driven domain wall motion dynamics. In contrast, whether skyrmions move toward $+y$ or $-y$ direction depends on the sign of skyrmion number Q . In our simulations, we get $Q = 1$ because the magnetization of the background FM layer points along $+z$ direction. Therefore, v_y is negative, which agrees

with the trajectories as shown in Fig. 3(a). Further, the skyrmion Hall angle θ_{sk} , which describes the deviation of skyrmions from x direction, is given by $\theta_{\text{sk}} = \text{atan}\left(\frac{v_y}{v_x}\right) = -\text{atan}\left(\frac{\alpha D}{G}\right)$. If the skyrmion radius R is larger than the domain wall width Δ , θ_{sk} can be well simplified to $-\text{atan}\left(\frac{\alpha R}{2\Delta}\right)$ [47]. Taking the parameters used in Fig. 3(a), θ_{sk} is estimated as -16° , corresponding well to the simulation results. When $D_1 \neq D_2$ and skyrmions are near the interface, F_i cannot be left out in Eq. (2). As illustrated in Fig. 7(c), F_i is positive if $D_1 < D_2$ and vice versa. From the expression of v_y , we can see that the skyrmion deflection can be changed by varying the magnitude of F_i and αDu . Once $D_1 < D_2$ and $F_i > \alpha Du$, skyrmions will move toward $+y$ direction. Otherwise, skyrmions still bend over $-y$ direction. The first proposed MUX is exactly based on this property.

In contrast, the Thiele equation for the SOT-driven case reads [32]:

$$\mathbf{G} \times \mathbf{v} - \alpha D \mathbf{v} + \mathbf{F}_{\text{SHE}} + \mathbf{F}_i = 0 \quad (3)$$

where $\mathbf{F}_{\text{SHE}} = F_{\text{SHE}} \hat{x}$ is the force induced by the SOT with magnitude F_{SHE} , the sign of which depends on the spin polarization direction σ . By solving Eq. (3), we can find

$$\begin{cases} v_x = \frac{\alpha D (F_{\text{SHE}} + F_i)}{G^2 + (\alpha D)^2} \\ v_y = \frac{G (F_{\text{SHE}} + F_i)}{G^2 + (\alpha D)^2} \end{cases} \quad (4)$$

If $D_1 < D_2$, F_{SHE} and F_i are both positive, thus the skyrmion Hall angle $\theta_{\text{sk}} = \text{atan}\left(\frac{v_y}{v_x}\right) = \text{atan}\left(\frac{G}{\alpha D}\right)$, which means that skyrmions can only bend toward $+y$ direction when approaching the interface from In_0 or In_1 . According to the expression of θ_{sk} , the skyrmion Hall effect should be remarkable in the SOT-driven case, agreeing well with the trajectories in Fig. 4(a). If $D_1 \geq D_2$, $F_{\text{SHE}} + F_i = 0$ can be achieved when skyrmions gradually approach the interface. Thereafter skyrmions remain static, as indicated by Fig. 7(a). Therefore, in the MUX displayed in Fig. 3(a) where the interface is along y direction, only Zhang-Li torque can be used to realize the MUX function.

If an oblique interface is introduced, as is the case in Fig. 4(a), \mathbf{F}_i can be expressed as $\mathbf{F}_i = (F_{ix}, F_{iy}, 0)$. Therefore, the solution to Eq. (3) becomes:

$$\begin{cases} v_x = \frac{\alpha D(F_{\text{SHE}} + F_{\text{ix}}) - GF_{\text{iy}}}{G^2 + (\alpha D)^2} \\ v_y = \frac{G(F_{\text{SHE}} + F_{\text{ix}}) + \alpha DF_{\text{iy}}}{G^2 + (\alpha D)^2} \end{cases} \quad (5)$$

To guide skyrmions move along the interface, we have $F_{\text{SHE}} > 0$, $F_{\text{ix}} < 0$ and $F_{\text{iy}} < 0$, i.e., $D_1 > D_2$. Assume that the interface encloses angle δ with the $-y$ direction, we have $k = \tan(\delta) = -\frac{v_x}{v_y} = \frac{F_{\text{iy}}}{F_{\text{ix}}}$. Subsequently, we can obtain:

$$F_i = -\frac{\alpha D + kG}{\alpha D\sqrt{1 + \delta^2}} F_{\text{SHE}} \quad (6)$$

Therefore, we can guide skyrmions motion along a designed interface when a proper SOT current is applied. Since F_i can also be generated at the interface where PMA changes, VCMA effect can be used to realize similar function, as shown in Fig. 4(b). Note that if the applied SOT current is too high, F_i provided by the interface may fail to satisfy Eq. (6). Under this circumstance, skyrmions can go through the electrode gated regions, resulting in wrong outputs.

B. Performance evaluation of SC implemented by skyrmionic logic devices

As shown above, we have successfully implemented SC by the skyrmionic logic devices. Despite the non-volatile advantage of skyrmion based devices, it is also necessary to evaluate the performance in terms of energy consumption, delay and area.

For the 8-bit stochastic multiplier, the energy consumption is about 1.264 pJ at $T = 0$ K (See Appendix D for energy calculation method), which is only about 5.5% of the CMOS based stochastic circuits [21]. In addition, the delay of our proposed skyrmionic stochastic multiplier is proportional to the SN, thus the whole delay of a N -bit SN stochastic multiplier is $N \times 19.6$ ns. In contrast, the delay of the CMOS based stochastic circuits is nonlinear, growing exponentially as the SN increases [21]. Consequently, when $\text{SN} > 12$, the delay of skyrmionic stochastic multiplier will become lower than that of CMOS based stochastic circuits, and the delay of skyrmionic stochastic multiplier will be extremely lower as the SN continually increases [21]. For example, when $\text{SN} = 20$, the delay of skyrmionic stochastic multiplier will be only 0.37% of that of the CMOS based stochastic circuits. In the meantime, the 8-bit stochastic adder

consumes about 1.224 pJ for 8-bit addition operation in about 137.6 ns, occupying about $0.6 \mu\text{m}^2$ for one device, which is competitive in terms of time efficiency and energy cost with typical CMOS based stochastic circuits. Considering also the higher thermal stability, the proposed skyrmionic logic devices demonstrate broad prospects as advanced alternatives to implement SC.

V. Conclusion

In this work, we propose a skyrmionic AND-OR logic device and two types of skyrmionic MUXs to implement SC. Thanks to the energy landscape designed by the VCMA effect or VCDMI effect, precise control of skyrmion-skyrmion collision is not required in our devices, thus enabling higher thermal stability. Based on the single-bit device, we further demonstrate an 8-bit stochastic multiplier and adder. Performance evaluation shows that our proposed skyrmionic logic devices outperform typical CMOS based circuits to execute SC in terms of energy consumption, time delay and area. Our work unfolds the great potential of skyrmionic logic devices to implement SC.

Appendix A: Simulation Methods

Micromagnetic simulations were performed by utilizing the GPU-accelerated simulation software mumax3 [48]. The dynamics at each site are depicted by the following Landau-Lifshitz-Gilbert (LLG) equation [4, 32]:

$$\frac{\partial \mathbf{m}}{\partial t} = -\gamma \mu_0 (\mathbf{m} \times \mathbf{H}_{\text{eff}}) + \alpha \left(\mathbf{m} \times \frac{\partial \mathbf{m}}{\partial t} \right) + \tau_{\text{SOT}} + \tau_{\text{CIP}}$$

where H_{eff} is the effective field, including the contributions from the anisotropy field, exchange field, DMI field, demagnetization field and thermal field (when $T \neq 0$ K).

$\mathbf{m} = \frac{\mathbf{M}}{M_s}$ is the reduced magnetization with M_s the saturation magnetization, α is the

damping constant, γ is the gyromagnetic ratio and μ_0 is the vacuum magnetic

permeability. $\tau_{\text{SOT}} = \gamma \frac{J_{\text{SOT}} \theta_{\text{SH}} \hbar}{2edM_s} (\mathbf{m} \times \boldsymbol{\sigma} \times \mathbf{m})$ denotes the SOT exerted on the

magnetization when applying a SOT current J_{SOT} with spin polarization direction $\boldsymbol{\sigma}$, spin Hall angle θ_{SH} , elementary charge e and FM layer thickness d and reduced Plank

constant \hbar [32, 49]. $\tau_{\text{CIP}} = u (\mathbf{m} \times \frac{\partial \mathbf{m}}{\partial x} \times \mathbf{m})$ is the exerted Zhang-Li torque when an

in-plane polarized current is applied, where $u = \gamma \frac{J_{\text{STT}} P \hbar}{2eM_s}$ with current density J_{STT} and

spin polarization P [32, 50].

Unless specified, the following material parameters are adopted in our simulations: exchange stiffness $A = 15 \text{ pJ} \cdot \text{m}^{-1}$, Gilbert damping $\alpha = 0.3$, saturation magnetization $M_s = 580 \text{ kA} \cdot \text{m}^{-1}$, spin polarization $P = 0.4$, spin Hall angle $\theta_{\text{SH}} = 0.4$, PMA constant of the FM layer $K_u = 0.8 \text{ MJ} \cdot \text{m}^{-3}$, DMI constant $D = 3.5 \text{ mJ} \cdot \text{m}^{-2}$ and VCMA coefficient $\xi = 48 \text{ fJ} \cdot \text{V}^{-1} \cdot \text{m}^{-1}$ [7, 29, 49]. The simulation area is divided into a cubic grid of $2 \text{ nm} \times 2 \text{ nm} \times 1 \text{ nm}$.

Appendix B: Skyrmionic AND-OR functions performed at $T = 250$ K

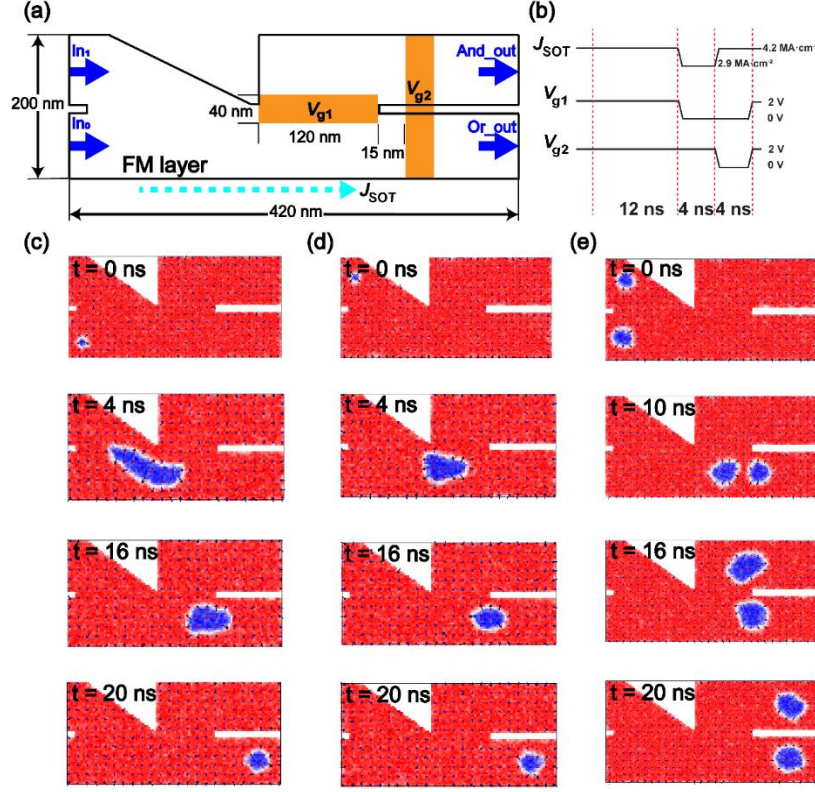


FIG. 6 Skyrmionic AND-OR logic device performed at $T = 250$ K: (a) the device structure is larger than the device in Fig.1(a). (b) Profile of J_{SOT} and electrode voltages. (c-e) Three cases of inputs and their corresponding simulation process and results.

We enlarge the area of the device and adjust timing diagram (see Fig. 6(a-b)) to enable the fluctuation of the skyrmions because of the high thermal stability of skyrmions in a wider racetrack [51]. Fig. 6(c-e) shows the simulation results with different inputs. The volume of skyrmion dramatically increases and fluctuating a lot at $T = 250$ K, which limits the current density applied in driving the skyrmions [52]. Basically, $J_{\text{SOT}} = 4.2 \text{ MA} \cdot \text{cm}^{-2}$ is applied to drive skyrmion motion but a lower current is used ($J_{\text{SOT}} = 2.9 \text{ MA} \cdot \text{cm}^{-2}$) when the second skyrmion moves to the AND lane. This is because the second skyrmion is more likely to crush at the edge while it fluctuates at $T = 250$ K compared to the situation at $T = 0$ K. The operation time becomes longer because of the larger size of the device as well as the lower driving current. But still, the AND-OR function can be achieved, indicating the high thermal stability of our device.

Appendix C: Simulation results of SOT-driven skyrmion motion at the interface where DMI changes

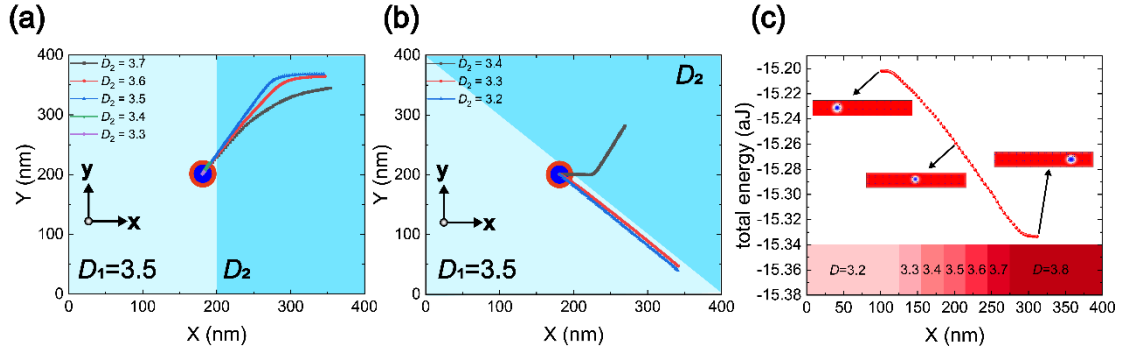


FIG. 7 (a-b) Trajectories of a SOT-driven skyrmion at different D_2 when an y -direction or oblique interface is introduced. $D_1 = 3.5 \text{ mJ}\cdot\text{m}^{-2}$ and $J_{\text{SOT}} = 4 \text{ MA}\cdot\text{cm}^{-2}$. (c) Effect of DMI on the energy of a nanotrack system. DMI strength increases from $3.2 \text{ mJ}\cdot\text{m}^{-2}$ at the left side to $3.8 \text{ mJ}\cdot\text{m}^{-2}$ at the right side, generating a force to drive the skyrmion along $+x$ direction. At each position, the energy of the system is recorded.

We investigate SOT-driven skyrmion motion at different interfaces where DMI changes. A constant SOT current $J_{\text{SOT}} = 4 \text{ MA}\cdot\text{cm}^{-2}$ is applied along $+x$ direction to drive skyrmion motion. As shown in Fig. 7(a) where the interface is exactly along y direction, skyrmion deflection is along $+y$ direction when $D_1 \leq D_2$. However, skyrmions will stop at the interface when $D_1 > D_2$. In contrast, in Fig. 7(b), we find that an oblique interface can guide skyrmions along $-y$ direction, which can be utilized to perform the MUX function. We further evaluate the effect of different DMI on the potential energy. We initialize a skyrmion at the left side of the nanotrack shown in Fig. 7(c). Along this nanotrack, the DMI strength D increases from $3.2 \text{ mJ}\cdot\text{m}^{-2}$ at the left side to $3.8 \text{ mJ}\cdot\text{m}^{-2}$ at the right side. Due to the DMI gradient, the skyrmion will move freely to the right side and the energy is measured at each position. We can see that the potential energy in the region with a lower DMI is higher, which can be used to guide the motion of skyrmions. Besides, the energy difference between two regions is nearly proportional to the DMI difference. By enlarging the DMI difference between two adjacent regions, we can regulate the skyrmion in a more stable manner, and a higher current can be used to drive the skyrmion.

Appendix D: Energy Consumption Evaluation Method

Energy consumed to operate an 8-bit stochastic multiplication is equal to 8 times of a single-bit AND operation according to the discussion above. For a single-bit AND operation, the energy consumption W for a constant SOT current J is calculated by

$$W = J^2 \cdot S_{\text{HM}} \cdot \rho \cdot l \cdot T,$$

where J is the current density flowing in the HM layer, S_{HM} is the y - z cross area of HM layer, ρ is the resistivity of the HM layer [53], l is the length of the HM layer in x direction and T is the time duration. According to the time diagram shown in Fig. 2(c), different current density J_i ($i = 1, 2, 3, 4$) is applied for different time duration T_i . The corresponding parameters are listed in the TABLE I.

Therefore, the energy consumed for a single-bit operation is about 158 fJ, which indicates the total energy consumed for 8-bit AND operation is $8 \times 158 = 1264$ fJ = 1.264 pJ. Similarly, the total power consumption for 8-bit MUX operation is calculated to be 1.224 pJ.

TABLE I. HM layer parameters for a single-bit AND operation

	J_i (MA·cm ⁻²)	S_{HM} (nm ²)	ρ (Ω·m)	l (nm)	T_i (ns)
i = 1	10	480	1.8×10^{-6}	2400	3
i = 2	20	480	1.8×10^{-6}	2400	0.6
i = 3	4.5	480	1.8×10^{-6}	2400	11
i = 4	10	480	1.8×10^{-6}	2400	5

References

- [1] S. Mühlbauer, B. Binz, F. Jonietz, C. Pfleiderer, A. Rosch, A. Neubauer, R. Georgii and P. Böni, Skyrmion lattice in a chiral magnet, *Science*. **323**, 915 (2009).
- [2] X. Z. Yu, N. Kanazawa, Y. Onose, K. Kimoto, W. Zhang, S. Ishiwata, Y. Matsui and Y. Tokura, Near room-temperature formation of a skyrmion crystal in thin-films of the helimagnet FeGe, *Nat. Mater.* **10**, 106 (2011).
- [3] R. Wiesendanger, Nanoscale magnetic skyrmions in metallic films and multilayers: a new twist for spintronics, *Nat. Rev. Mater.* **1**, 1 (2016).
- [4] W. Kang, Y. Huang, X. Zhang, Y. Zhou and W. Zhao, Skyrmion electronics: an overview and outlook, *Proc. IEEE*. **104**, 2040 (2016).
- [5] Y. Zhou, E. Iacocca, A. A. Awad, R. K. Dumas, F. C. Zhang, H. B. Braun and J. Åkerman, Dynamically stabilized magnetic skyrmions, *Nat. Commun.* **6**, 8193 (2015).
- [6] S. Tacchi, RE Troncoso, M. Ahlberg, G. Gubbiotti, M. Madami, J. Åkerman and P. Landeros, Interfacial Dzyaloshinskii-Moriya Interaction in Pt/CoFeB Films: Effect of the Heavy-Metal Thickness, *Phys. Rev. Lett.* **118**, 147201 (2017).
- [7] X. Zhang, Y. Zhou, M. Ezawa, G. P. Zhao, and W. Zhao, Magnetic skyrmion transistor: skyrmion motion in a voltage-gated nanotrack, *Sci. Rep.* **5**, 11369 (2015).
- [8] S. Luo, M. Song, X. Li, Y. Zhang, J. Hong, X. Yang, X. Zou, N. Xu, and L. You, Reconfigurable Skyrmion Logic Gates, *Nano Lett.* **18**, 1180 (2018).
- [9] X. Zhang, M. Ezawa, and Y. Zhou, Magnetic skyrmion logic gates: conversion, duplication and merging of skyrmions, *Sci. Rep.* **5**, 9400 (2015).
- [10] S. Luo, Y. Zhang, M. Shen, J. O-Yang, B. Yan, X. Yang, S. Chen, B. Zhu, and L. You, Skyrmion-based high-frequency signal generator, *Appl. Phys. Lett.* **110**, 112402 (2017).
- [11] W. Kang, C. Zheng, Y. Huang, X. Zhang, Y. Zhou, W. Lv, and W. Zhao, Complementary skyrmion racetrack memory with voltage manipulation, *IEEE Electron Device Lett.* **37**, 924 (2016).
- [12] D. Zhu, W. Kang, S. Li, Y. Huang, X. Zhang, Y. Zhou, W. Zhao, Skyrmion Racetrack memory with random information update/deletion/insertion, *IEEE Trans.*

[Electron Devices](#). **65**, 87 (2018).

- [13] X. Chen, W. Kang, D. Zhu, X. Zhang, N. Lei, Y. Zhang, Y. Zhou and W. Zhao, Complementary skyrmion racetrack memory enables voltage-controlled local data update functionality, [IEEE Trans. Electron Devices](#). **65**, 4667 (2018).
- [14] Y. Liu, N. Lei, C. Wang, X. Zhang, W. Kang, D. Zhu, Y. Zhou, X. Liu, Y. Zhang, and W. Zhao, Voltage-driven high speed skyrmion motion in a skyrmion-shift device, [Phys. Rev. Appl.](#) **11**, 014004 (2019).
- [15] G. Finocchio, F. Büttner, R. Tomasello, M. Carpentieri and M. Kläui, Magnetic skyrmions: from fundamental to applications, [J. Phys. D: Appl. Phys.](#) **49**, 42 (2016).
- [16] R. Tomasello, E. Martinez, R. Zivieri, L. Torres, M. Carpentieri and G. Finocchio, A strategy for the design of skyrmion racetrack memories, [Sci. Rep.](#) **4**, 6784 (2014).
- [17] B. R. Gaines, Stochastic computing systems, [Advances in Information Systems Science](#). **37** (1969).
- [18] W. Poppelbaum, C. Afuso and J. Esch., Stochastic computing elements and systems, in *Proc. AFIPS Spring Joint Computer Conference, 1967*, p. 635.
- [19] B. R. Gaines, Stochastic computing, in *Proc. AFIPS Spring Joint Computer Conference, 1967*, p. 149.
- [20] Y. Ding, Y. Wu and W. Qian, Generating multiple correlated probabilities for MUX-based stochastic computing architecture, in *Proc. ICCAD, San Jose, CA, USA, 2014*, p. 519.
- [21] J. M. de Aguiar and S. P. Khatri, Exploring the viability of stochastic computing, in *IEEE International Conference on Computer Design (ICCD), New York, 2015*, p. 391.
- [22] R. Venkatesan, S. Venkataramani, X. Fong, K. Roy and A. Raghunathan, SPINTASTIC: Spin-based Stochastic Logic for Energy-efficient Computing, in *Proc. Design, Automation & Test in Europe Conference & Exhibition (DATE), 2015*, p. 1575.
- [23] M. Chauwin, X. Hu, F. Garcia-Sanchez, N. Betrabet, C. Moutafis and J. S. Friedman, Conservative skyrmion logic system, [arXiv:1806.10337](#).

- [24] A. Alaghi and J. Hayes, Survey of stochastic computing, [ACM Trans. Embed. Comput. Syst.](#) **12**, 1 (2013).
- [25] W. Jiang, P. Upadhyaya, W. Zhang, G. Yu, M. B. Jungfleisch, F. Y. Fradin, J. E. Pearson, Y. Tserkovnyak, K. L. Wang, O. Heinonen, S. G. E. te Velthuis and A. Hoffmann, Blowing magnetic skyrmion bubbles, [Science](#). **349**, 283 (2015).
- [26] G. Yu, P. Upadhyaya, X. Li, W. Li, S. K. Kim, Y. Fan, K. L. Wong, Y. Tserkovnyak, P. K. Amiri and K. L. Wang, Room-Temperature Creation and Spin-Orbit Torque Manipulation of Skyrmions in Thin Films with Engineered Asymmetry, [Nano Lett.](#) **1981** (2016).
- [27] G. Yu, P. Upadhyaya, Y. Fan, J. G Alzate, W. Jiang, K. L Wong, S. Takei, S. A Bender, Li-Te Chang, Y. Jiang, M. Lang, J. Tang, Y. Wang, Y. Tserkovnyak, P. K. Amiri and K. L Wang, Switching of perpendicular magnetization by spin-orbit torques in the absence of external magnetic fields, [Nat. Nanotech.](#) **9**, 7 (2014).
- [28] W. Skowroński, T. Nozaki, Y. Shiota, S. Tamaru, K. Yakushiji, H. Kubota, A. Fukushima, S. Yuasa and Y. Suzuki, Perpendicular Magnetic Anisotropy of Ir/CoFeB/MgO trilayer system tuned by electric fields, [Appl. Phys. Express.](#) **8**, 53003. (2015).
- [29] T. Nozaki, A. Koziol-Rachwal, W. Skowronski, V. Zayets, Y. Shiota, S. Tamaru, H. Kubota, A. Fukushima, S. Yuasa, and Y. Suzuki, Large voltage-induced changes in the perpendicular magnetic anisotropy of an MgO-based tunnel junction with an ultrathin Fe layer, [Phys. Rev. Appl.](#) **5**, 044006 (2016).
- [30] C. Ma, X. Zhang, J. Xia, M. Ezawa, W. Jiang, T. Ono, S. N. Piramanayagam, A. Morisako, Y. Zhou and X. Liu, Electric field-induced creation and directional motion of domain walls and skyrmion bubbles, [Nano Lett.](#) **353** (2019).
- [31] W. Zhang, H. Zhong, R. Zang, Y. Zhang, S. Yu, G. Han, G. L. Liu, S. S. Yan, S. Kang and L. M. Mei, Electrical field enhanced interfacial Dzyaloshinskii-Moriya interaction in MgO/Fe/Pt system, [Appl. Phys. Lett.](#) **113**, 122406 (2018).
- [32] J. Sampaio, V. Cros, S. Rohart, A. Thiaville and A. Fert, Nucleation, stability and current-induced motion of isolated magnetic skyrmions in nanostructures, [Nat. Nanotech.](#) **8**, 839 (2013).

- [33] R. Sbiaa, H. Meng and S. N. Piramanayagam, Materials with perpendicular magnetic anisotropy for magnetic random access memory, [Phys Status Solidi-R. **5**, 413 \(2011\).](#)
- [34] J. Iwasaki, M. Mochizuki and N. Nagaosa, Current-induced skyrmion dynamics in constricted geometries, [Nat. Nanotech. **8**, 742 \(2013\).](#)
- [35] X. Zhang, G. P. Zhao, H. Fangohr, J. P. Liu, W. X. Xia, J. Xia and F. J. Morvan, Skyrmion-skyrmion and skyrmion-edge repulsions in skyrmion-based racetrack memory, [Sci. Rep. **5**, 7643 \(2015\).](#)
- [36] W. Jiang, X. Zhang, G. Yu, W. Zhang, X. Wang, M. B. Jungfleisch, J. E. Pearson, X. Cheng, O. Heinonen, K. L. Wang, Y. Zhou, A. Hoffmann and S. G. E. te Velthuis, Direct observation of the skyrmion Hall effect, [Nat. Phys. **13**, 162 \(2016\).](#)
- [37] K. Litzius, I. Lemesh, B. Krüger, P. Bassirian, L. Caretta, K. Richter, F. Büttner, K. Sato, O. A. Tretiakov, J. Förster, R. M. Reeve, M. Weigand, I. Bykova, H. Stoll, G. Schütz, G. S. D. Beach and M. Kläui, Skyrmion Hall effect revealed by direct time-resolved X-ray microscopy, [Nat. Phys. **13**, 170 \(2016\).](#)
- [38] G. Chen, Spin-orbitronics: Skyrmion Hall effect, [Nat. Phys. **13**, 112 \(2017\).](#)
- [39] N. Nagaosa and Y. Tokura, Topological properties and dynamics of magnetic skyrmions, [Nat. Nanotech. **8**, 899 \(2013\).](#)
- [40] J. Zang, M. Mostovoy, J. H. Han and N. Nagaosa, Dynamics of Skyrmion Crystals in Metallic Thin Films, [Phys. Rev. Lett. **107**, 136804 \(2011\).](#)
- [41] M. Raí, M. Jeroen, S. Clecio and M. Milorad, Deflection of (anti)ferromagnetic skyrmions at heterochiral interfaces, [Phys. Rev. B. **99**, 104409 \(2019\).](#)
- [42] A. Caprile, M. Pasquale, M. Kuepferling, M. Coisson, T. Y. Lee and S. H. Lim, Microwave Properties and Damping in [Pt/Co] Multilayers With Perpendicular Anisotropy, [IEEE Magn. Lett. **5**, 1 \(2014\).](#)
- [43] M. B. Karadeniz and M. Altun, Sampling based random number generator for stochastic computing, *IEEE International Conference on Electronics, Circuits and Systems (ICECS), Batumi, 2017*, p. 227.
- [44] D. Pinna, F. Abreu Araujo, J.-V. Kim, V. Cros, D. Querlioz, P. Bessiere, J. Droulez and J. Grollier, Skyrmion Gas Manipulation for Probabilistic Computing, [Phys.](#)

[Rev. Appl. 9, 064018 \(2018\).](#)

- [45] D. Vodenicarevic, N. Locatelli, A. Mizrahi, J. S Friedman, A. F Vincent, M. Romera, A. Fukushima, K. Yakushiji, H. Kubota, S. Yuasa, S. Tiwari, J. Grollier and D. Querlioz, Low-Energy Truly Random Number Generation with Superparamagnetic Tunnel Junctions for Unconventional Computing, [Phys. Rev. Appl. 8, 054045 \(2017\).](#)
- [46] A. Thiaville, Y. Nakatani, J. Miltat and Y. Suzuki, Micromagnetic understanding of current-driven domain wall motion in patterned nanowires, [Europhys. Lett. 69, 990 \(2005\).](#)
- [47] A. Hrabec, J. Sampaio, M. Belmeguenai, I. Gross, R. Weil, S.M. Che'rif, A. Stashkevich, V. Jacques, A. Thiaville and S. Rohart, Current-induced skyrmion generation and dynamics in symmetric bilayers, [Nat. Commun. 8, 15765 \(2017\).](#)
- [48] A. Vansteenkiste, J. Leliaert, M. Dvornik, F. Garcia-Sanchez and B. Van Waeyenberge, The design and verification of Mumax3, [AIP Adv. 4, 107133 \(2014\).](#)
- [49] X. Zhang, Y. Zhou and M. Ezawa, Magnetic bilayer-skyrmions without skyrmion Hall effect, [Nat. Commun. 7, 10293 \(2016\).](#)
- [50] S. Zhang and Z. Li, Roles of Nonequilibrium Conduction Electrons on the Magnetization Dynamics of Ferromagnets, [Phys. Rev. Lett. 93, 127204 \(2004\).](#)
- [51] X. Chen, W. Kang, D. Zhu, X. Zhang, N. Lei, Y. Zhang, Y. Zhou and W. Zhao, Skyrmion dynamics in width-varying nanotracks and implications for skyrmionic applications, [Appl. Phys. Lett. 111, 202406 \(2017\).](#)
- [52] L. Kong and J. Zang, Dynamics of an insulating skyrmion under a temperature gradient, [Phys. Rev. Lett. 111, 067203 \(2013\).](#)
- [53] P. F. Carcia, Perpendicular magnetic anisotropy in Pd/Co and Pt/Co thinfilm layered structures, [J. Appl. Phys. 63, 5066 \(1988\).](#)